Fall 2018

Modulated photothermal radiometry: Detector sensitivity study and experimental setup

Jessica Nicole Seals

Department:

MODULATED PHOTOTHERMAL RADIOMETRY: DETECTOR SENSITIVITY STUDY AND EXPERIMENTAL SETUP

by

JESSICA NICOLE SEALS

A THESIS

Presented to the Faculty of the Graduate School of the

MISSOURI UNIVERSITY OF SCIENCE AND TECHNOLOGY

In Partial Fulfillment of the Requirements for the Degree

MASTER OF SCIENCE

IN

NUCLEAR ENGINEERING

2018

Approved by:

Dr. Joseph Graham, Advisor
Dr. Joshua P Schlegel
Dr. Ayodeji Alajo

ABSTRACT

This thesis outlines the development of a system used for determining the surface thermal diffusivity of both non-irradiated and irradiated materials. The motivation for this work is to establish a modulated photothermal radiometry (PTR) system on the campus of Missouri University of Science and Technology. One of the main efforts described in this thesis is the design and construction of the physical apparatus. Along the way, it was necessary to perform a detailed sensitivity analysis of the system to determine whether the expected signal emitted from the sample falls within the bounds of detectivity for the HgCdTe (MCT) detector used to measure the infrared (IR) emission of the specimen.

The power of IR radiation from an idealized planar specimen surface was calculated based on the power of the incident laser used to modulate heat flux into the surface. The analysis performed was based on the principles of the radiative heat transfer from the specimen surface and heat conduction within the specimen. Upon comparing the calculated values to those provided by a thermoelectrically cooled HgCdTe detector, it was determined that while a 400 mW laser should produce an emission signal strong enough for the detector to measure, the DC voltage response of a thermoelectrically cooled MCT detector falls below the measurement range of the lock-in amplifier used in the signal path. These finding were used to inform a second stage redesign of the system which incorporates a new laser and liquid nitrogen cooled MCT detector.

This work summarizes the initial design, construction and troubleshooting of an in-house PTR system that helps establish a pathway to a fully complete and working system.

ACKNOWLEDGMENTS

First and foremost I would like to thank my advisor, Dr. Joseph Graham, for his patience and wisdom during this process. Wtithout him this would not have been possible, and one could not hope for a better advisor. I would also like to thank Dr. Joseph Graham, Dr. Hyoung Lee and the Nuclear Regulatory Commision for providing the financial opportunity to complete this work.

Finally, I would like to thank my family and friends. Without this support system, I surely would have failed. I am forever grateful to all of you for encouraging me to flourish and chase my dreams.

TABLE OF CONTENTS

Page

APPENDICES

LIST OF ILLUSTRATIONS

Page

LIST OF TABLES

Page

1. INTRODUCTION

Materials exposed to ionizing radiation are subject to structural alterations in ways that can sometimes negatively affect their material properties. As neutrons bombard a solid, the atomic structure of the material becomes saturated with point defects, causing the material's microstructure to change and extended defects to be introduced. One type of property alteration of great importance to nuclear fission and fusion systems is the degradation of thermal properties governing the rate of heat transfer through the material. The objective of the modulated photothermal radiometry (PTR) technique is to determine how this rate of heat transfer is modified by measuring the thermal diffusivity at its surface. In the context of radiation effects studies, surface thermal diffusivity is important in connection to accelerated ageing and radiation damage experiments using ion beams.

Energetic heavy ions produced in a particle accelerator, though highly effective at producing high displacement damage doses in a short period of time, are not highly penetrating. They may produce tens to hundreds of displacements per atom (dpa) in a matter of hours compared to years of exposure in a fission or fusion system. However, the limited range of heavy energetic ions, being on the order of several microns typically, complicates post-irradiation analysis by conventional materials characterization techniques designed for bulk materials. In short, the effects of high dpa displacement damage may only be seen at the materials surface. This requires the use of surface specific materials characterization techniques. Modulated PTR represents one such technique that is also non-contact and non-destructive.

When a material is exposed to radiation, material degradation can include changes in mechanical, electronic, optical, chemical and thermal properties, the latter of which includes thermal diffusivity, the focus of the PTR technique. Every solid has an atomic structure, which for crystalline solids is composed of a lattice decorated with atoms. As a material is exposed to radiation, some high energy particles can affect the atomic structure by causing atoms to be displaced from their lattice site, as seen in Figure 1.1. This phenomenon of knock-on damage produces primary and secondary knock-on atoms (PKAs and SKAs), and ultimately quasi-stable pairs of point defects known as Frenkel pairs. A Frenkel pair comprises a self-interstitial atom (SIA) and a lattice vacancy [1].

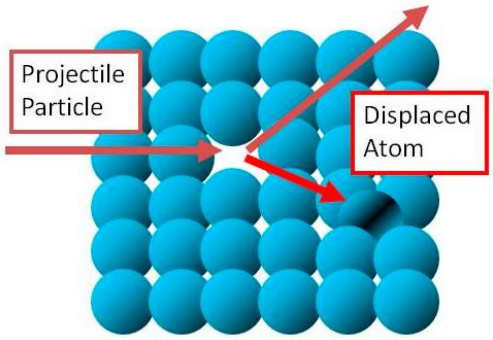

Figure 1.1: Displacement of an atom, creating a defect in the lattice structure. [2]

The production of point defects from the radiation damage cascade of atomic displacements can accumulate, diffuse, interact with each other, recombine or grow into extended defects such as clusters, dislocations, voids, precipitates and bubbles. All of these extended defects can contribute to changes in the properties of materials. As materials in high temperature, high radiation environments are constantly exposed to these changes, it is important to note how that affects materials of interest. One can anticipate that changes, either positive or negative will occur continuously over the

lifetime of a nuclear reactor. One of the major challenges in designing nuclear systems is to accurately design around and predict these changes given a dose, temperature, stress state and other environmental stressors. For example, multiphysics modeling of nuclear reactors requires databases of material properties. If such databases do not reflect the changes in properties brought about from irradiation damage, the models are of limited predictive value. It therefore becomes necessary to determine these material parameters using comprehensive material models or experimental measurements.

Thermal properties of particular importance in reactor design and modeling include thermal conductivity, heat capacity, and thermal diffusivity, though the three are interrelated. Thermal conductivity is a measure of a material's ability to conduct heat. In metals, it depends on the concentration and mobility of free electrons in the material and decreases with temperature, except at cryogenic temperatures where its behavior follows the heat capacity [3]. In nonmetals – materials with an electronic bandgap – thermal conductivity depends largely on lattice vibrations at low temperatures while electrons only begin to conduct heat at high temperatures [3]. For this reason, the thermal conductivity of insulators and semiconductors tend to exhibit more complex temperature dependence.

Heat capacity is the amount of added heat necessary to change the temperature of a substance [4]. This value determines, among other things, how much a material must be heated to raise its temperature to the point where infrared radiation begins to make a significant contribution to heat transfer. Lastly, the thermal diffusivity is the rate of heat transfer through a material and it is dependent on both the thermal conductivity and heat capacity [5].

These values are typically tabulated for unirradiated materials used in nuclear applications but often the data is incomplete or missing for the same materials under a particular combination of dpa, temperature, and stress. Furthermore, novel nuclear materials synthesized as composites, coatings and nanostructured materials can have widely varying properties, even within the same composition. Designing nuclear systems with new materials requires a combination of detailed, physics-based predictive models as well as high-throughput experimental studies over a wide matrix of doses and environmental conditions. The high-throughput approach is made possible by combining ion beam irradiations with surface characterization techniques such as PTR.

PTR allows one to determine which materials are best suited for high temperature, high radiation environments based on the coefficient of thermal diffusivity, α, of non-irradiated and irradiated samples as a function of temperature and dose. The change in these values will determine how a material's ability to transfer heat changes through the lifetime of a nuclear power plant or facility.

1.1. EXISTING DIFFUSIVITY MEASUREMENT TECHNIQUES

There are numerous methods to determine the thermal diffusivity of a material. One of the most common methods is the flash method, which uses a pulse of energy, either from a laser or flash lamp, to heat the surface of a sample. The temperature is measured on both the front surface and rear surface of the sample and is used to calculate the diffusivity [6]. This method only allows for the thermal characterization of bulk samples of a singular, homogenous material. In contrast, PTR can be used to determine

thermal characteristics of materials with multiple layers, including layers of different materials such as thin coatings.

The transient hot bridge (plane source) method is another method used in determining the thermal transport properties of materials. This method uses two halves of a sample with a probe sandwiched between them. The probe acts as both the heat source and temperature sensor during this process and as current is applied to the probe, the sample surface rises in temperature [3]. The temperature of the sample increases as a function of time and can be used to determine thermal properties of the material.

Like PTR, the 3ω method can also be used to determine the thermal diffusivity in thin films. In 3ω, a material is periodically heated using a resistive line heater driven at angular frequency ω, causing heating at a frequency 2ω that also induces a temperature response with a 2ω component, the amplitude and phase of which are associated with the materials layer structure and layer compositions. The oscillation causes the heater resistance to oscillate at 2ω as well, which when convolved with the initial drive frequency of ω, generates a 3ω signal. This 3ω signal is then used to calculate the thermal conductivity and diffusivity [8].

A large error for thermal property measurements comes from the contact necessary with the sample. Modulated Photothermal Radiometry is different from other thermal characterization techniques in that it is non-contact, non-destructive, thin film surface characterization technique. The method uses the measurement of heat radiated from the material surface to determine its thermal diffusivity.

Because the measurement is taken from IR emission at the surface of the material, this technique does not require alteration to the state of the material for analysis. The

surface of a material in a high temperature, high radiation environment receives the highest amount of energy from particles that strike the material before traveling through it. This method allows the coatings on the surface of a material to be studied, along with layered materials.

1.2. MODULATED PHOTOTHERMAL RADIOMETRY

Modulated Photothermal Radiometry is an optical system that operates as follows:

1. A modulated light source, most often a laser, is used to heat the surface of a sample.
2. The diffusion of heat into the surface layer(s) induces a modulation frequency amplitude response and phase lag in the surface temperature.
3. The sample then emits heat in the form of infrared radiation.
4. This emission is then collected with a high-speed, high sensitivity infrared detector.

In Figure 1.2, it is shown that the laser passes through several optical components before heating the sample surface. The optical isolator is used to ensure that laser light does not reflect back into the laser. Interference from the laser with itself can lead to power instabilities and non-linear behavior. The chopper is used to rapidly modulate the laser signal. It consists of a rotating wheel with sectors of alternating transparent and optically dense material. A splitter cube is used to direct a portion of light into a visible light photodetector to create a reference signal for calculations. After passing through a narrow aperture of a parabolic mirror, the laser light shines incident onto the surface of the sample.

Modulated laser heating causes the sample to rise in temperature and emit heat, which is then collected, redirected and recondensed on an infrared detector using parabolic mirrors. One parabolic mirror collects IR light from its focal point, the laser spot. The mirror shape redirects the light as a parallel beam onto another parabolic mirror which recondenses the light into a focal point located on the surface of an IR detector.

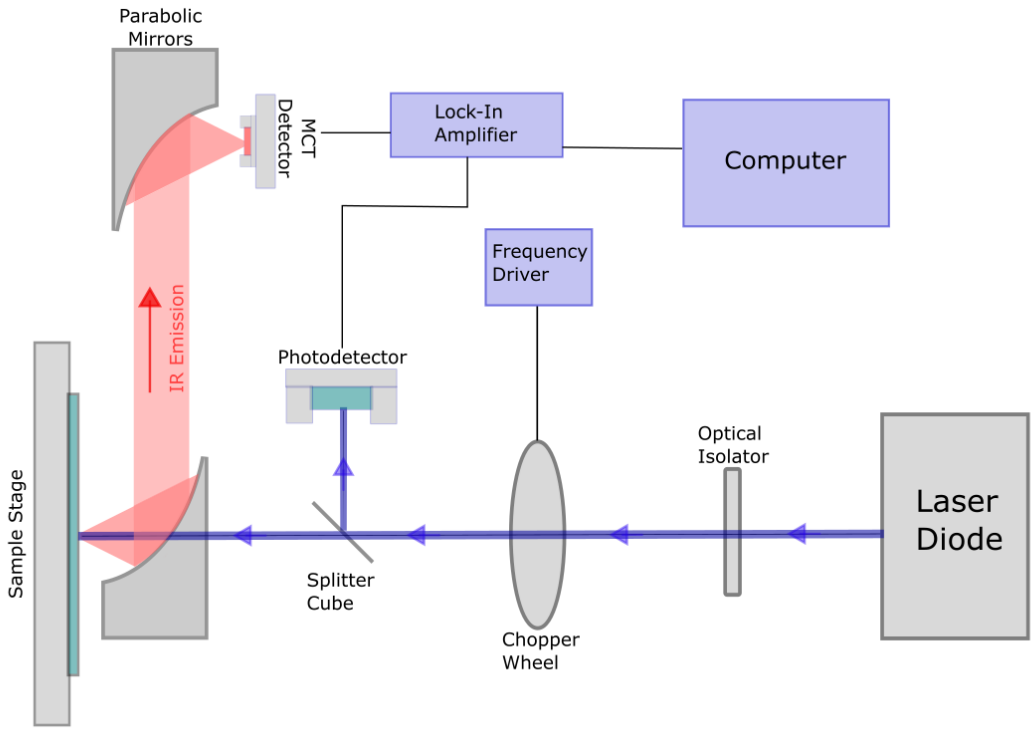

Figure 1.2: Modulated photothermal radiometry apparatus.

The IR detector is a mercury cadmium telluride (MCT, HgCdTe) type detector. The MCT detector material acts as a photoresistor sensitive to IR photons. When an increased flux of incident IR power is incident on a voltage-biased photoresistive material, the resistance drops permitting the detector preamplifier to read a change in current and output a proportional voltage. This voltage therefore contains information

about changes in IR flux. Because IR radiation is naturally present in the ambient environment of the lab, other, often much larger signals are usually present in the signal output. A constant background IR signal coming from the average room temperature environment results in a DC signal. This signal can be rejected by AC coupling the detector or by implementing a bias offset. IR noise in the system is more problematic as it can overwhelm the IR signal from the specimen. An effective approach for dealing with this is to process the signal with a lock-in amplifier which amplifies weak signals of a specific frequency. The frequency is determined by a modulated reference signal or an internal oscillator. The detector signal thus passes through a lock-in amplifier along with the reference from the visible light photodetector. Both the amplitude and phase lag (with respect to reference) of the IR light are measured by the lock-in amplifier.

When a material is heated with a modulated source, it produces an emission modulated at the same frequency as the source, though possibly phase delayed. The frequency-domain response of phase and amplitude of the emission contains information specific to the thermal diffusivities and layer thicknesses of the layered specimen. The frequency response can be predicted from the method of thermal quadrupoles or by direct integration of the heat equation. For a single thin layer, a qualitative argument can be made to demonstrate the basic frequency response. When the thermal diffusion length is comparable to the thickness *d* of a thin layer, then the frequency dependence of phase and amplitude will vary rapidly when

$$f \sim \frac{\alpha}{\pi d^2} \tag{1}$$

If the layer thickness is known, then the approximate diffusivity of the layer can be inferred by, for example, identifying the frequency where the phase changes most quickly. For more accurate determination, a model must be fit to experimental data. The objective of this study is to take the concept of modulated photothermal radiometry and assemble, align, and test optical components to create a system that is capable of thermal diffusivity measurements. This process includes performing sensitivity calculations to ensure the laser power will be sufficient for creating a temperature rise in the sample that is sufficient in producing an emission that can be seen by all detecting components. Based on this analysis, a selection of optimal detector and laser power can be made with which to build the system.

In the past, PTR had been performed to determine thermal characteristics of a variety of thin film materials such as diamond films [9], GaAs wafers [10], as well as bruise age determination [11]. The samples analyzed in this work include inorganic solids such as 316 stainless steel, whose properties are known and can be used to calibrate the system.

In 1979, Per-Erik Nordal and Svein Otto Kanstad presented a mathematical model of PTR response. A mathematical expression for the temperature rise of the surface of a sample, the amplitude of temperature variations associated with the frequency, and the radiant emittance associated with the varying heat signal were presented [12]. These mathematical models helped to frame some calculations in this work. Nordal and Kanstad used the Modulated Photothermal Radiometry to determine the absorption spectra of K_2SO_4 [12].

2. EXPERIMENTAL SETUP

2.1. EQUIPMENT SETUP AND PROCEDURE

The system was built on a Newport Integrity 1 optical table system, featuring threaded holes fitting ¼-20 screws, allowing each component to be fastened down to prevent movement. The table also has a 3.4 mm skin with an integrated dampened layer that attenuates a 10-50 Hz range of floor vibrations, preventing them from disturbing sensitive equipment and promoting consistency in measurements. The optical system itself is housed in a custom-made enclosure of light absorbing medium and 25mm anodized aluminum rails, shown in Figure 2.1. The black foamboard protects the system from light entering that could distort results and also acts as safety enclosure to protect lab users from the laser light. The hinged lid on the front of the enclosure allows easy access to components inside of the enclosure for repositioning, alignment, and staging of the samples, and closes easily to ensure accurate results during trials.

Figure 2.1: Light-proof enclosure for optical components.

The light path of components inside the enclosure begins with a multi-mode laser diode emitting a signal with a wavelength of 404 nm. The signal is provided by a 400 mW blue laser diode inside of a Thorlabs thermo-electric cooled laser diode mount as seen in Figure 2.2. The mount is situated atop a tip, tilt, and rotation stage that allows the laser beam to be aligned with respect to the optical table and optical components. The stage has a tip/tilt adjustment range of ±5º, and a rotation adjustment range of ±10º. Because of the large beam divergences of laser diodes, laser collimation is accomplished by means of an aspheric lens.

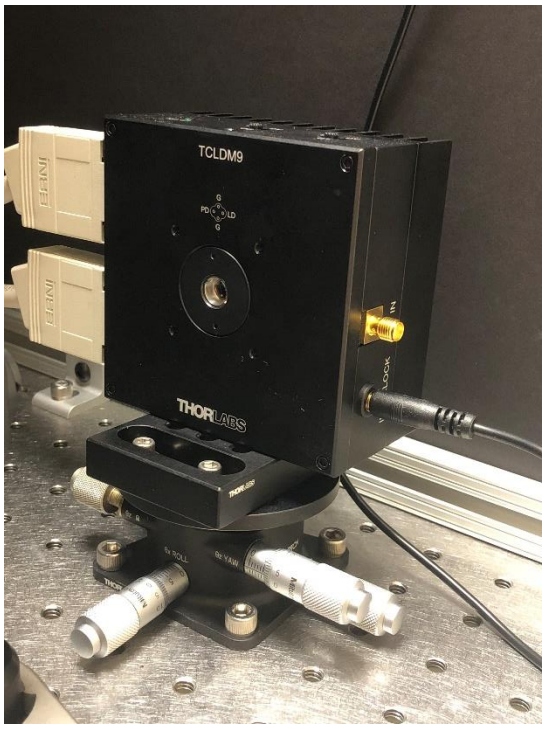

Figure 2.2: Laser diode mount and tip, tilt, and rotation stage.

Attached to the side of the laser diode mount is an interlock that prevents the system from being operational should the door of the cage be opened while the laser is

energized. When the lid is opened, a depressed interlock switch is released and immediately cuts power to the laser diode mount. The interlock can be seen in Figure 2.3.

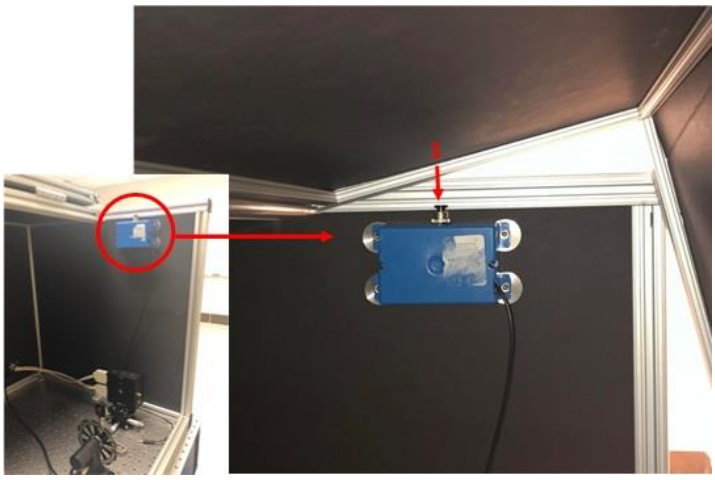

Figure 2.3: Momentary contact switch for laser interlock.

The laser power is controlled by two components: the laser diode controller and the temperature controller, shown in Figure 2.4.

Figure 2.4: Laser diode controller (top) and temperature controller (bottom).

The laser diode controller (LDC) and temperature controller (TC) work in tandem to operate the laser diode. The LDC can drive the laser in constant current or constant power mode. Constant current mode holds the current to the laser at a specific, steady value while constant power mode compensates for fluctuating current to hold the laser diode at a steady power. The thermoelectric temperature controller precisely controls the temperature for the laser diode. This helps to stabilize the wavelength, reduce noise, and tune the wavelength and modulation of wavelength by regulating the temperature [21].

The laser passes from the diode mount through a polarization-dependent optical isolator, which minimizes feedback into the optical components. The laser enters the isolator at 0º, parallel to the table surface, aligned with the laser's plane of polarization, and exits the isolator vertically polarized.

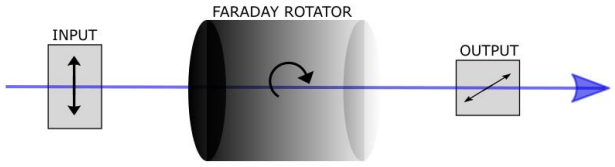

Figure 2.5: The light enters the faraday rotator at 0º relative to the y axis. The faraday rotator uses a magnetic field to rotate the axis of polarization by 45º.

The plane of polarization is also rotated 45º by a Faraday Rotator, which uses a magnetic field to rotate the axis of polarization. As a result, the new plane of polarization is 45º, relative to the table surface. The faraday rotator concept can be seen in Figure 2.5 and the optical isolator in Figure 2.6.

Figure 2.6: Optical isolator.

Then, the signal passes through an optical chopper, Figure 2.7. The chopper creates a pulsed signal from a continuous beam [22]. It has a 50% duty cycle. As the blades of the chopper block the signal, the material being analyzed experiences a brief cooling period. Inversely, as the light passes through the windows in the chopper, the material experiences a brief heating period during each window. The optical chopper is driven at a specified frequency that can vary from 20Hz-1kHz. This frequency is chosen manually in the control software, which will be discussed in further detail in this section.

Following the chopper, the signal passes through a non-polarizing beamsplitter cube, Figure 2.8, which directs 10% of the signal into a photodetector, Figure 2.9. The detection of the light produces a signal that acts as a reference for measuring the phase of the infrared emission output in the lock-in amplifier.

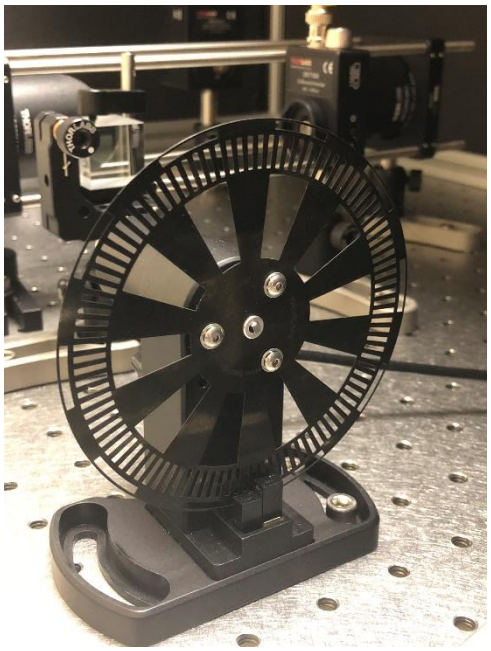

Figure 2.7: Optical chopper.

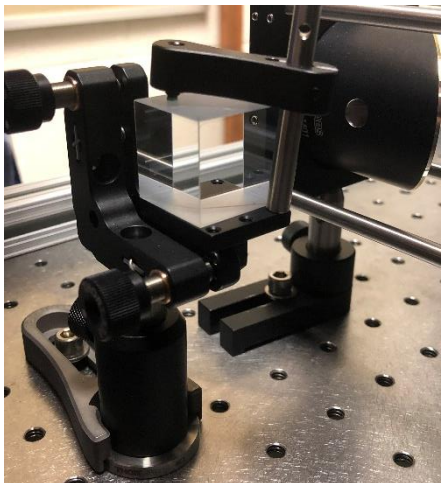

Figure 2.8: Beamsplitter cube in housing apparatus.

The photodetector is a silicon biased detector from ThorLabs. It is designed for the detection of signals in the range of 200nm to 1100nm [23]. It can be operated in one of two modes, photoconductive or photovoltaic. Photoconductive mode applies a reverse bias, and the measured output current is linearly proportional to the input optical power

[23]. The photodiode is zero biased in photovoltaic mode, utilizing the photovoltaic effect. As the current in the device is restricted, a voltage accumulates with exposure to radiant energy. For this system, the detector is operated in photoconductive mode.

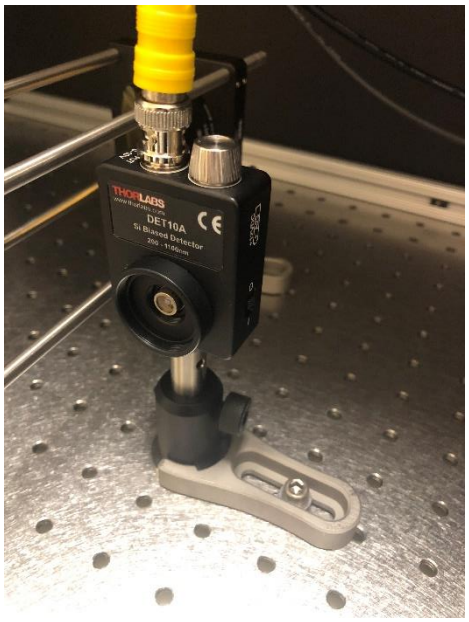

Figure 2.9: Silicon biased photodetector.

The laser diode beam terminates at the surface of the sample. At this point, the sample is heated by the laser and radiated infrared light. The sample is mounted on a Thorlabs XYZ translation stage using double sided tape, shown in Figure 2.10. Eventually the sample stage can be replaced with a variable temperature stage for thermal diffusivity measurements at low and high temperatures.

This emission is then collected in a closed pair of gold coated 90º off-axis parabolic mirrors, shown in Figure 2.11, that direct the signal into an infrared detector.

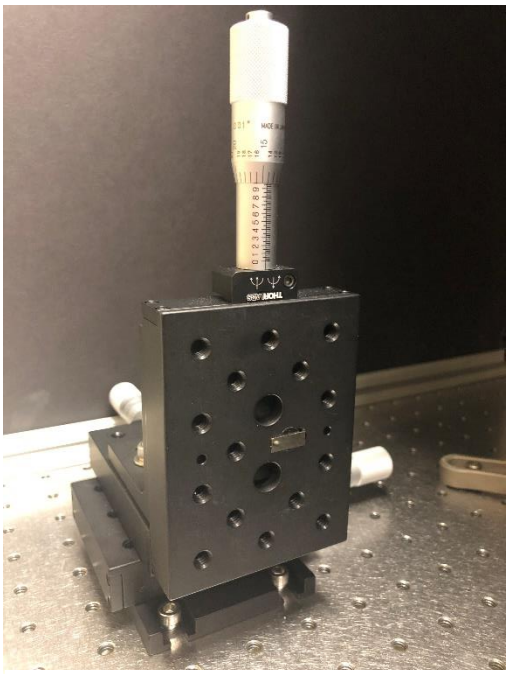

Figure 2.10: XYZ translation stage.

The first mirror contains a centered hole parallel to the beam, allowing the beam to travel through the mirror to reach the sample surface. The entry point for the beam can be seen in Figure 2.12. An advantage of this geometry is that the mirror focal point must fall along the beam axis, obviating the need to align focal point and beam spot in three dimensions.

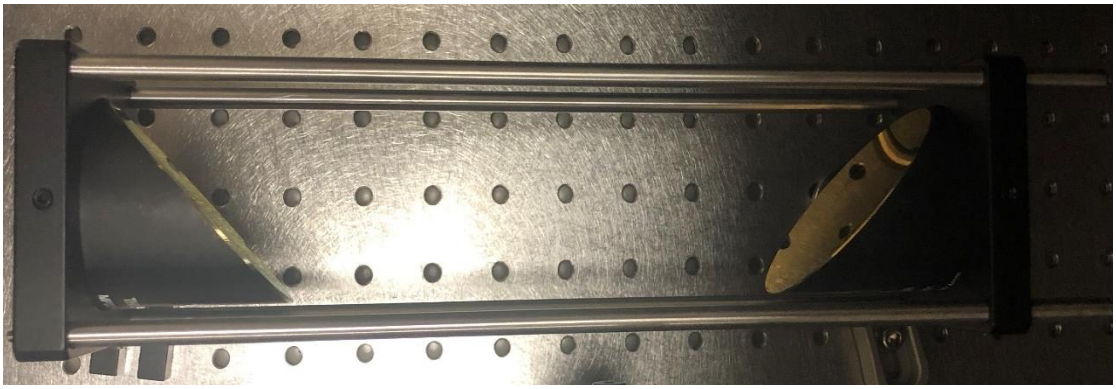

Figure 2.11: Off-axis parabolic mirrors.

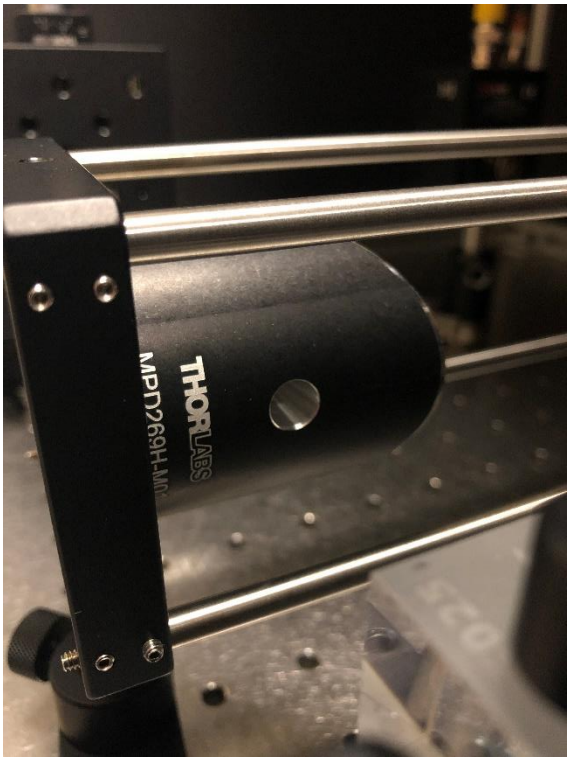

Figure 2.12: Off-axis parabolic mirror with centered hole for alignment beam.

The beam travels through the mirror, exits at the center of the gold-coated surface, and strikes the sample. The hole that the beam travels through has a diameter of 3mm on the coated surface, and 8mm on the back of the mirror, shown in Figure 2.12. The beam size, once it reaches the sample surface, is then 3mm in diameter or smaller. The mirrors have a focal length of 152.4 mm (6”), so they must be positioned at the appropriate distance both from the sample stage, and from the infrared detector. The mirrors are distanced approximately 225 mm apart, measured from the center of the parabolic mirror. Once the sample is heated, additional infrared photons are emitted towards the coated surface of the mirror and reflected directly towards the second mirror that does not have a

centered hole. This second mirror focuses the IR light into the active area of the infrared detector. The IR detector can be seen in Figure 2.13.

Figure 2.13: Mercury cadmium telluride IR Detector.

The amplified MCT detector is thermo-electrically cooled and features switchable-gain and switchable-bandwidth. Thermo-electric cooling allows for a higher detectivity than a room temperature detector, resulting in a lower output offset and higher gain. The AC coupling of the detector requires a chopped or pulsed input signal in the wavelength range of 2.0-5.4µm. The gain can be set between 0-40dB, in 6dB steps, and the bandwidth can be set in one of eight steps from 1.25-160kHz. The active detection area is 1mm x 1mm, so it is essential that the detector be positioned at an accurate distance from the mirror for the signal to be detected with minimal geometric attenuation losses.

From the MCT detector, the voltage signal passes through a lock-in amplifier. Initially, a second hand single channel lock-in amplifier was used in tandem with an oscilloscope to ensure that the amplifier could lock-in to the photodiode reference. Once it was established that the signal had the correct shape, amplitude and frequency using the oscilloscope in Figure 2.14, it was used as a reference for the Stanford Research Systems SR510 single channel lock-in amplifier in Figure 2.14.

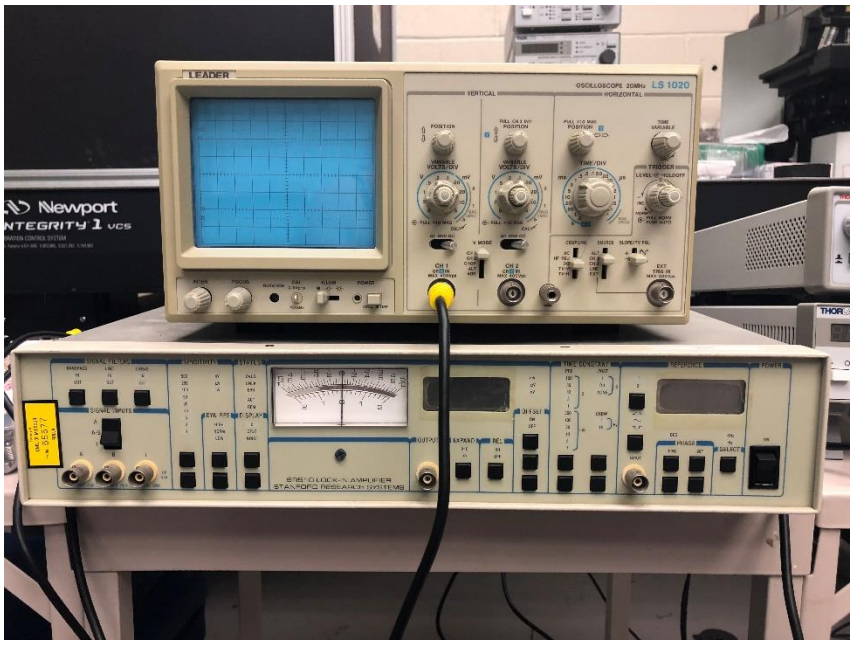

Figure 2.14: Oscilloscope (top) and single channel lock-in amplifier (bottom).

The single channel lock-in amplifier (LIA) is a phase and amplitude sensitive amplifier that operates by multiplying two AC input signals to generate a DC output proportional to the cross modulation amplitude. Though the phase lag cannot be directly measured, the reference signal can be manually phase shifted to determine the phase lag

by optimizing the cross modulation amplitude. One of these signals is a reference signal with a specific phase. In this system, the reference signal is coming from the photodetector that detects the signal that is directed toward it from the splitter cube. This signal is a chopped beam with a user specified frequency. Once the LIA uses this to create a reference signal, it will multiply it by the second signal, the voltage output of the MCT detector.

LabView software is used to control the electronic test equipment and hardware controllers, as well as analyze data that is output from the lock-in amplifier. Figure 2.15 shows a capture of this program for the single channel LIA.

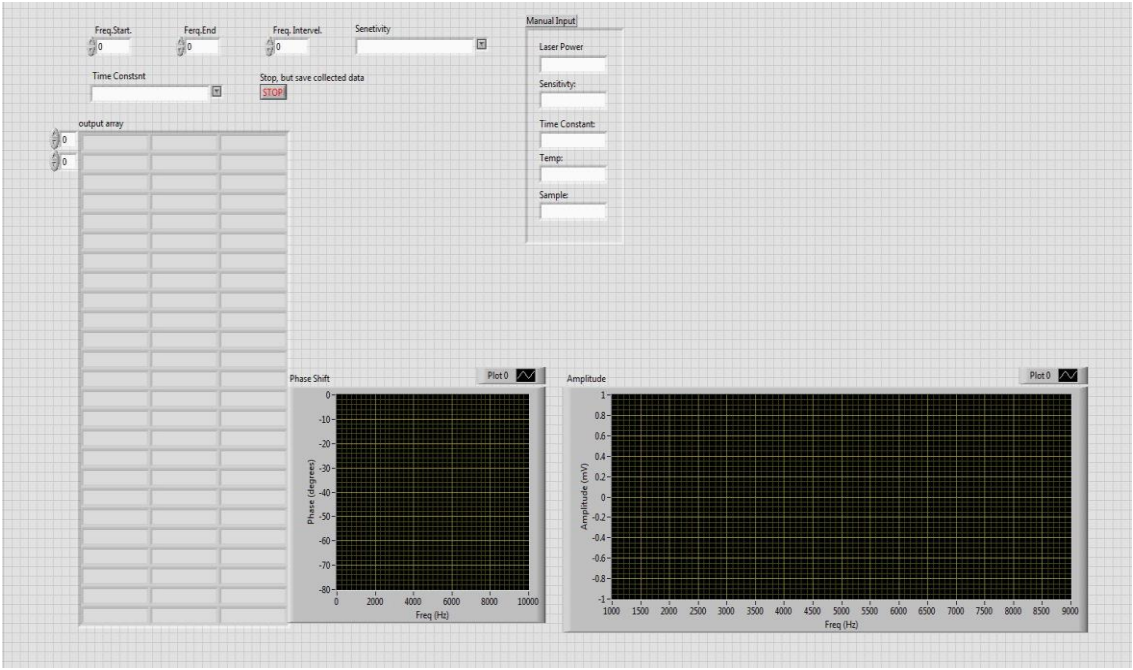

Figure 2.15: Capture of LabView program used for a single channel LIA system.

Certain measurement parameters, such a laser power, sensitivity scale and time constant for the LIA, temperature, and name of the sample are entered manually into user

interface. The LIA values set the LIA amplitude range setting during operation. The user enters a frequency start value is entered, followed by a frequency end point value and interval. This will tell the chopper control unit what frequency to start the copper at, what frequency to end at, and how many steps to take in between those two values. In other words, it defines the data range of the measurements.

The LabView program operates sequentially. After the laser power is switched on, and the program is initiated, the program steps through chopper frequencies, measuring the LIA response and recording values before incrementing to the next chopper frequency. At the first frequency step, a reference is generated by the LIA at that specific frequency. Once the sample's IR response is measured, the LIA the analyzes the signal. It records the phase delay of the IR signal with respect to the reference and record this value. It also multiplies the two signals and records the amplitude. Once this sequence is complete, and all values are recorded, the LabView program will instruct the chopper to increase to the next frequency indicated, and the process will repeat until the frequency end value is reached.

The program then uses the measured values to generate two graphs. The first, on the left side of Figure 2.16, plots the phase shift (degrees) vs. frequency (Hz). This will be used to determine at which frequencies the phase shifts most rapidly. The second, on the right side of Figure 2.16, plots the signal amplitude (mV) vs. frequency (Hz). This plot visualizes the amplitude roll-off. When the phase shift of the two signals is zero degrees, the two signals are in phase. When this occurs, the multiplication of the signals will generate a maximum amplitude. These two curves will be fit to an existing model for

amplitude and phase vs frequency in order to determine the coefficient of thermal diffusivity.

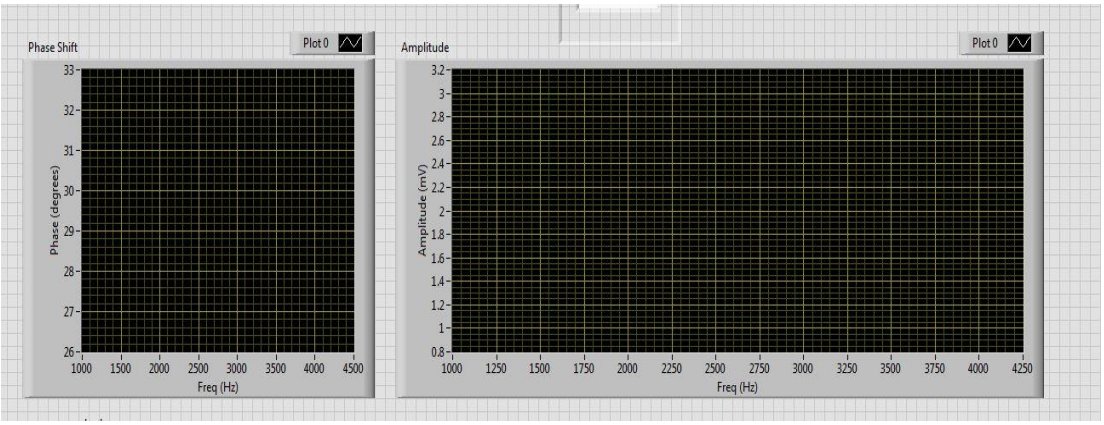

Figure 2.16: Capture of plots generated in LabView.

2.2. UPDATES AND CHANGES

In the first version of the system, the chopper was replaced with an electro-optic modulator (EOM). In an EOM, a voltage is applied across two lithium niobate crystals, inducing a change in the axis of polarization and a phase delay in the signal. The modulator uses the halfwave voltage to vary the intensity of a beam from maximum to minimum intensity. A control voltage is amplified with a a high voltage amplifier to produce the input for controlling the EOM. This allows, for example, the wave produced to have a sine wave shape with a phase dependent on the voltage applied. As the modulator was being aligned in the system, the signal was not being varied, and in turn not producing a sine wave.

During troubleshooting, it was determined that the modulator may have required the use of either an input polarizer, output polarizer, or even both. The polarizers would

have been used to rotate the axis of polarization of the beam to the necessary angle for input and output to and from the modulator. Once they were introduced to the system and positioned both before and after the modulator, the signal still appeared as a steady beam, rather than the fluctuating sine wave. This may be related to the nature of the laser beam. EOMs are designed for single mode lasers could suffer in performance when used with multimode lasers. For this reason, the electro-optic modulator was replaced with an optical chopper. The principal of their operation is the same, to rapidly vary the intensity of the beam. With the optical chopper, a rapidly spinning wheel with evenly spaced transparent and optically thick sectors modulate the signal as a square wave with a 50% duty cycle. Besides the fact that beam choppers can only modulate laser power as a square wave, they are typically more limited in frequency range.

After aligning the system with the 400 mW laser, no signal could be measured with the MCT detector. It was assumed that either the laser was not powerful enough to sufficiently heat the sample or the detector was not sufficiently sensitive, though in either case proper alignment is still necessary to give the best results. To resolve the uncertainty about where the problem(s) lie, calculations, to be discussed in the modeling section, were performed in order to determine what sensitivity was theoretically possible for a properly functioning system with the given components. A measurement of the laser power also confirmed that the laser diode was not operating near its 400 mW nominal power and was assumed to have been damaged at a point in the mounting process. As a result, a new 400 mW, 405 nm from a different manufacturer was purchased.

A Stanford Research dual phase lock-in amplifier (SR830) replaced the single channel amplifier (SR510). This LIA displays both the magnitude and phase of a signal

and utilizes digital signal processing. Using this LIA eliminates steps in the process of determining the phase and amplitude of the infrared signal. The dual phase LIA is able to simultaneously record both phase and amplitude simultaneously. With a single channel LIA, the phase must be determined by measuring cross modulation over all phase lags. The LabView integration of the dual channel LIA is therefore much simpler. The only difference in the two programs, is that the dual phase LIA program lacks an output array of values.

3. THEORY AND MODELING

3.1. BACKGROUND

In order to determine the threshold of the detector and the power of the signal being emitted from the sample surface, analytical calculations of the modulated heating and light analysis were performed. Firstly, the power of the light incident on the MCT detector surface had to be determined. From this value, it could be use to determine how much laser power would be necessary to heat the sample surface or, conversely, how responsive a detector was required for the given laser power and geometric losses.

An object that absorbs all incident radiation upon it and re-emits that energy is referred to as a blackbody. A perfect blackbody is a perfect absorber, and in turn a perfect emitter [13]. Because materials emit a portion of incident radiation, they are referred to as graybodies. Graybodies are distinguished from blackbodies by a reduced radiance accounted for by their emissivity [13].

A blackbody of temperature T radiating from a flat surface has a spectral radiance, B_ν described by Planck's law

$$B_\nu(\nu, T) = \frac{2h\nu^3}{c^2}\frac{1}{e^{h\nu/kT} - 1} \tag{2}$$

where ν is the frequency of emitted light, h is the Planck constant, c is the speed of light, and k is the Boltzmann constant. When integrated over all wavelengths, this gives the radiance

$$L = \int B_\nu(\nu, T)d\nu = \frac{2\pi^4 k^4}{15c^2h^3}T^4 = \frac{\sigma}{\pi}T^4 \tag{3}$$

where σ is the Stefan-Boltzmann constant. The angular dependence of the radiant intensity of a blackbody emitting from a planar surface follows Lambert's cosine law

$$L(\theta, \phi) = L \cos\theta \tag{4}$$

By integrating over the solid angle **Ω**, where θ and ϕ are the polar and azimuthal angles measured with respect to the surface normal. The radiant emittance, j^* becomes

$$j^* = \int_0^{2\pi} \int_0^{\pi/2} L(\theta, \phi) d\Omega = L \int_0^{2\pi} d\phi \int_0^{\pi/2} \cos\theta \sin\theta \, d\theta \tag{5}$$

$$j^* = \pi L = \sigma T^4 \tag{6}$$

which is nothing more than the Stefan-Boltzmann law. A blackbody has emissivity ε=1. All graybody materials will have an emissivity of ε<1. Taking this into consideration, the radiant emittance for a graybody can now be written as

$$j^* = \varepsilon\sigma T^4 \tag{7}$$

In light of the fact that the IR light collected by the PTR system uses parabolic mirrors and a detector with a responsivity dependent on wavelength, it is appropriate to modify the above integrals by introducing the solid angle limits of integration into the spectral intensity

$$I(\nu, T, \theta, \phi) = \frac{2h\nu^3}{c^2} \frac{\cos\theta}{e^{h\nu/kT} - 1} \tag{8}$$

Given that the responsivity parameters are typically given in terms of wavelength and

$$\nu = \frac{c}{\lambda} \tag{9}$$

it follows that

$$I(\lambda, T, \theta, \phi) = \frac{2hc^2}{\lambda^5} \frac{\cos\theta}{e^{hc/\lambda kT} - 1} \tag{10}$$

The incident power on the detector is given by

$$P = A\varepsilon \int_0^{2\pi} \int_0^{\theta_m} \int_0^{\infty} I(\lambda, T, \theta, \phi) d\lambda \sin\theta \, d\theta d\phi = A\varepsilon g j^* \tag{11}$$

where A is the area of the emitting region collected by the parabolic mirrors, i.e. the laser spot. Because of the finite size of the laser spot, the comparatively smaller size of the detector's active area, and imprecisions in the mirror optics and detector location, a geometric loss factor g can also be included. Assuming that the detector size is the limiting factor for light collection, we will assume $A = 1\ \text{mm}^2$ for subsequent analysis.

Equation 12 includes the geometry factor, with A representing the area of the beam, *a* representing the major axis of the mirror, *b* the minor axis, and *R* the focal length of the off-axis parabolic mirrors.

$$g = \frac{ab}{4R^2} \tag{12}$$

With this expression it becomes possible to estimate the IR power flux into the detector for a given sample surface temperature and mirror collection geometry. Next, it becomes necessary to relate fluctuations in the surface temperature to the radiant emittance. When a sample is heated by a continuous wave laser modulated by a chopper, the power signal follows a pulse wave time dependence with frequency and duty cycle determined by the chopper mask pattern and rotation speed. The signal is a square wave for a 50% duty cycle. While the unblocked laser irradiates the sample, the sample surface is heating. Subsequently, as the light is blocked by the chopper, the sample experiences a brief cooling period. This heating and cooling cycle produce a temperature change ΔT with each cycle. It is worth noting that the time averaged temperature of the sample surface is governed by the time averaged laser power and substrate thermal conductivity. Averaging the modulations over many cycles, the temperature of the sample will rise

from its initial ambient temperature to a plateau from the average beam heating. Superimposed on the plateau will be small temperature variations from the modulated heat source. The temperature will continue to oscillate about this plateau as the light passes through and is blocked by the windows of the rapidly spinning optical chopper.

The time-dependent temperature, T, considers the constant mean (or background) temperature of the sample T_0 at the plateau and the time-dependent change in temperature ΔT after heating, so that

$$T = T_0 + \Delta T \tag{13}$$

Substituting Equation 13 into Equation 6, expanding to first order in ΔT, the radiant emittance is now

$$j^* \approx \varepsilon\sigma(T_0^4 + 4\Delta T T_0^3) \tag{14}$$

Note that higher order terms of the temperature modulation are dropped. Except at low cryogenic temperatures, $\Delta T << T_0$. Thus the emittance can be treated as approximately proportional to the temperature oscillations. This equation can be used to find the radiant emittance of the sample after being heated by the laser. Continuing, j^* substituted into Equation 11 gives the change in incident power into the detector active area:

$$P = Agj^* \approx Ag\varepsilon\sigma(T_0^4 + 4\Delta T T_0^3) \tag{15}$$

$$P \approx Ag\varepsilon\sigma T_0^4 + Ag\varepsilon\sigma T_0^4 \frac{4\Delta T}{T_0} \tag{16}$$

$$\Delta P = Ag\varepsilon\sigma T_0^4 \frac{4\Delta T}{T_0} \tag{17}$$

3.2. MODELING

Once the power incident on the detector surface was determined, the next step was is to predict the time dependence of the surface temperature. As a first approximation, one can assume that all laser power incident on the sample surface is absorbed at the surface. For metallic samples, it is a good approximation to assume that all power absorbed is absorbed at the surface owing to the shallow penetration depth of visible light in metals. On the other hand, the assumption of perfect absorption is not entirely justified. A certain portion of visible light is reflected off a polished surface, especially in metals. Many metals, however have a low spectral reflectance at 405 nm. Thus this approximation is reasonable for order of magnitude analysis with the given choice of laser. The calculation of the time dependence of the surface temperature was performed using a MATLAB script. The temperature was predicted using integration of the heat equation. The distribution of heat, or temperature variance, in a given sample over time can be given by the heat equation below:

$$\rho c_p \frac{\partial T}{\partial t} = k\nabla^2 T + \dot{q_v} \tag{18}$$

And can be rewritten as

$$\partial_t \mathrm{T} = \alpha \partial_x^2 \mathrm{T} + \frac{\dot{q_v}}{\rho c_p} \tag{19}$$

where $\alpha = \frac{k}{\rho c_p}$ is the thermal diffusivity, ρ represents the mass density of the material, c_p is the specific heat capacity at constant pressure, k is the thermal conductivity, T is the temperature, and $\dot{q_v}$ is the volumetric heat source term. Using Equation 18 as the starting point, it can then be discretized in time using the forward differencing method to obtain Equation 19 and its boundary conditions:

$$\frac{T_{i+1,j} - T_{i,j}}{\Delta t} = \alpha_j \, \partial x^2 T_{i,j} + \frac{\dot{q}_{v,i,j}}{(\rho C_p)_j} \tag{20}$$

$$\dot{q}_{v,i,j} = \begin{Bmatrix} \dot{q}_{0,1} & j = 1 \\ 0 & j > 1 \end{Bmatrix} \tag{21}$$

The meaning of the boundary conditions is that, in the first layer, all laser power is absorbed. In terms of the laser power, the heat source term is

$$\dot{q}_{0,j} = \frac{P_i}{A_{beam} * \Delta x} \tag{22}$$

where P_i is the power of the laser at time step i and Δx is the thickness of the first layer of material. For any layer not equal to j=1, the heat source term is equal to zero. Equation 18 can now be discretized in space using a diamond differencing scheme to obtain the following:

$$\partial_x^2 T_{i,j} = \frac{T_{i,j+1} - 2T_{i,j} + T_{i,j-1}}{\Delta x^2} \tag{23}$$

Equation 23 can now be substituted back into Equation 20 , resulting in Equation 24:

$$\frac{T_{i+1,j} - T_{i,j}}{\Delta t} = \alpha_j \frac{T_{i,j+1} - 2T_{i,j} + T_{i,j-1}}{\Delta x^2} + \frac{\dot{q}_{v,i,j}}{(\rho C_p)_j} \tag{24}$$

Rearranging, Equation 24 now becomes:

$$T_{i+1,j} = T_{i,j} + \alpha_j \Delta t \frac{T_{i,j+1} - 2T_{i,j} + T_{i,j-1}}{\Delta x^2} + \frac{\dot{q}_{v,i,j}}{(\rho C_p)_j} \tag{25}$$

$$\frac{\alpha_j \Delta t}{\Delta x^2} < 0.5 \tag{26}$$

The von Neumann stability criterion, Equation 26, was used to check the stability of the differencing schemes used in the partial differential equations above. As long as

this is satisfied, the numerical scheme of the calculations will be stable. When this criterion is not satisfied, truncation errors will grow exponentially.

This equation was implemented as a MATLAB script to determine the temperature change in the first layer of a hypothetical sample with a typical thermal properties and hence the radiant emission source term. Because the method can be used on multilayered materials, the code can be initialized to include layers of various materials. The sample being used for modeling, however, was a single homogenous layer of stainless steel 316. After sufficiently many layers, the temperature of the sample is assumed to remain at a constant room temperature, T_0. In other words, a Dirichlet boundary condition was used to represent substrate as a semi-infinite heat sink at a constant ambient temperature.

Also, because of the way the code was written, adiabatic conditions were imposed on the surface. The first layer of the material was considered to be a vacuum, and assigned the temperature in the vacuum layer to match that of the surface of the sample. The surface of the sample is treated as the second layer of material for computational convenience.

The code was able to provide an estimated ΔT of the material. It is known that T_0 is approximately equal to the room temperature in Kelvin. Predicting ΔT allowed calculations to be performed that would ensure the sample was heated sufficiently in order to generate a signal that could be detected by the infrared detector.

The surface temperature of the laser heated specimen was also compared to an analytical model and compared with the numerical calculations in MATLAB. The

intensity of the laser beam was calculated, using the equation below where P_{laser} is the power of the laser and r is the radius of the laser beam in meters.

$$I_0 = \frac{P_{laser}}{\pi r^2} \tag{27}$$

The change in temperature can be estimated using Equation 28

$$\Delta T_0 = \frac{I_0 l}{2\mathrm{k}} \tag{28}$$

where l is the thickness of the sample and k is the conductivity of the sample [1]. After performing this calculation, the change in temperature was equal to 0.001 K. This calculation confirmed the value found in the MATLAB code for the change in temperature of the SS316 sample. The confirmation of this value helped to verify the values found while calculating the radiant emittance and power from the sample. The values used in and found during these calculations can be seen in Table 3.1.

Table 3.1: Values used in calculating laser beam intensity.

I_0	ρC_p	ΔT	l
28294.21 W/m^2	3.868×10^6 J/m^3-K	0.001 K	$1 \times 10^{-6} m$

3.3. INSTRUMENT LIMITATIONS

Using data provided for the HgCdTe amplified photodetector by ThorLabs, calculations were performed to determine the detector's capacity to detect the emission signal from the sample, and whether or not the small AC voltage output would be detectable by the lock-in amplifier above noise. Once the power of the signal incident on

the detector is calculated, it can be compared to the equipment parameters to determine whether it is within the capability of the detector and LIA to read the emission.

The voltage response of the detector measuring a steady-state black body is

$$V = G \times A \int_0^{2\pi} \int_0^{\theta_m} \int_0^{\infty} R(\lambda) I(\lambda, T, \theta, \phi) d\lambda \sin\theta \, d\theta d\phi \tag{29}$$

G is the detector gain. θ_m is the acceptance polar angle of the collection parabolic mirror.

$$\theta_m = \arctan\frac{1}{6} = 0.165 \text{ rad} = 9.46° \tag{30}$$

Upon substitution of this value into Equation 29,

$$V = 0.085 \times G \times A \int_0^{\infty} R(\lambda) I(\lambda, T) d\lambda \tag{31}$$

As neither the wavelength dependence of Planck's law nor the detector responsivity changes much within a 1 μm neighborhood of the detector peak, it is useful to estimate the contribution to the detector response from the IR light in a 1 μm spectral range about the detector peak

$$dV_{peak} \approx 0.085 \times G \times A \times R_{peak} \times I_{peak}(T) \times 10^{-3}\text{mm} \tag{32}$$

Table 3.2 contains estimates of the voltage response for two different MCT detectors. The original thermoelectric-cooled Thorlabs detector and a liquid nitrogen cooled MCT from Teledyne Judson technologies.

Since these values only include a portion of the IR spectrum they underestimate to total voltage response. However, the AC coupling effectively cancels out the large DC component from the background of ambient IR light. Evidently, only the AC signal – the change in voltage due to the laser modulation - is relevant for estimating signal strength into the lock-in amplifier.

Table 3.2: Comparing peak voltage response of each detector.

Detector	Judson J15D16	Thorlabs PDA10JT
Peak Wavelength [μm]	11	4.75
Maximum Gain [V/V]	500	100
R_{peak} [V/W]	3000	300
I_{peak}(300 K) [W mm^{-3}]	0.01	0.002
I_{peak}(500 K) [W mm^{-3}]	0.06	0.12
dV_{peak} $(300\ K)$	1.2V	5mV
dV_{peak} $(500\ K)$	7.4V	300mV

From before

$$P \approx A\varepsilon\sigma T_0^4 + A\varepsilon\sigma T_0^4 \frac{4\Delta T}{T_0} \tag{33}$$

$$\Delta P = A\varepsilon\sigma T_0^4 \frac{4\Delta T}{T_0} \tag{34}$$

It follows that

$$\Delta dV_{peak} = dV_{peak} \frac{4\Delta T}{T_0} \tag{35}$$

Of course, ΔT, calculated from the MATLAB script depends on the material's thermal properties, the thickness of the surface layer(s) and the modulation frequency. Below are values for typical peak voltages expected from samples with a 0.001K ΔT.

Given that the lower limit of the SR510 lock-in amplifier is 100 nV, at room temperature, the ThorLabs detector falls outside of the capabilities of the LIA, and is not suitable for ambient measurements. The newer SR830 model has a sensitivity limit of 2 nV, seen in Table 3.3. However, given additional geometric, reflectance, graybody and laser power losses, it is likely that measurements with the ThorLabs detector will be

noisy at best. At high temperatures, measurements with the ThorLabs detector should be possible, but with losses, may be noisy. The Judson detector values fall well within the SR510 lock-in amplifier range of 100 nV-500 mV, and within the SR830 range of 2 nV-1V, making it suitable for both ambient and high temperature measurements. In Figure 3.1, the peak responsivity and intensity vs wavelength can be seen. The figure shows that as the wavelength of the signal increases, the Judson detector has a higher responsivity associated with increasing wavelength than the Thorlabs detector.

Table 3.3: Comparing calculated voltage response due to IR signal.

Detector	ΔT (K)	ΔdV_{peak} (300K)	ΔdV_{peak} (500K)
Judson J15D16	0.001 K	16 µV	59.2 µV
Thorlabs PDA10JT	0.001 K	6.67 nV	2400 nV

From the preceding analysis, the incident power was found to be sufficiently small enough that the corresponding relative output voltage is well below the limitations of the MCT photodetector and lock-in amplifier combination. The graph in Figure 3.2 shows the values provided by Thorlabs for the responsivity vs power of the detector. Using this graph, and the numerical approach, it is now known that the signal is within the limits of the Thorlabs MCT detector parameters. Using the values provided by Teledyne Judson, however, the J15D12 is more suitable for the environment in which testing will take place.

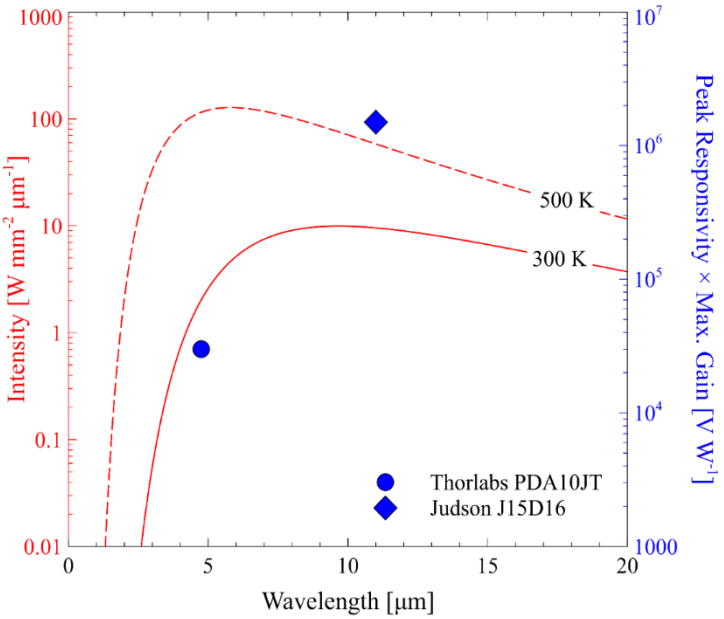

Figure 3.1: Peak responsivity and intensity vs wavelength for both MCT detectors.

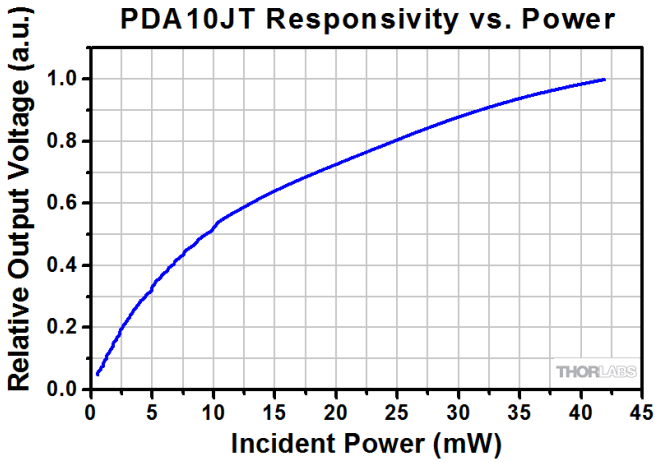

Figure 3.2: Responsivity vs power of Thorlabs MCT detector.

The Teledyne Judson Mercury Cadmium Telluride (HgCdTe or MCT) photoconductive detector is designed to operate in the 2-26µm wavelength range. In Table 3.4, there are some comparative values between the ThorLabs PDA10JT and the Judson JD15D12 MCT detectors. The Teledyne Judson detector is more sensitive than

the Thorlabs detector and is able to generate a voltage that can be detected by the lock-in amplifier, an essential step in the process. These values make the Teledyne Judson detector a more ideal fit for this system.

Table 3.4: Comparative values for each detector.

Detector	Peak Wavelength @ I_{peak}	Peak D*	Typical Responsivity
Judson J15D16	>12 µm	$3 \times 10^{10}\ cm \cdot Hz^{\frac{1}{2}}/W$	3000 V/W at Peak Wavelength
Thorlab PDA10JT	4.8 µm	~$1.48 \times 10^{10}\ cm \cdot Hz^{\frac{1}{2}}/W$	300 V/W at Peak Wavelength

4. RESULTS

Using the equations and analysis described previously, and specifications provided by ThorLabs and Teledyne Judson technologies, the following calculations were performed: the ability of the ThorLabs MCT photodetector to measure a quantifiable IR emission from the sample, the ability of the Stanford Research Systems lock-in amplifier to detect the voltage from the photodetector, and whether the power of the laser was high enough to sufficiently heat the sample.

Table 4.1: Values used in calculations.

Material	Frequency, f, v	Stefan-Boltzmann Constant, σ	Diffusivity of unirradiated SS316, D	Thermal Conductivity of unirradiated SS316, k
SS316	100 Hz	5.67×10^{-8} $W/m^2\text{-}K^4$	3.4978×10^{-6} m^2/s	13.53 $W/m\text{-}K$

Included in Table 4.1 are the values that remained constant throughout calculations. Table 4.2 includes values for a sample of unirradiated stainless steel 316 (SS316). The SS316 has known values, and for this reason it was chosen to align and test the system, and to ensure the equipment was producing accurate results.

Table 4.2: Calculated power incident on detector for SS316 sample.

Material	Emissivity	ΔT	j*	Min Detector Power	Power Entering Detector
SS316	0.28	0.00107 K	117.26 W/m^2	8.32×10^{-9} W	8.9×10^{-7} W

The area of sample being heated is equivalent to the size of the beam hitting the sample. Because the beam passes through the off-axis parabolic mirror with a diameter of 1 mm^2, it is assumed the heating area, and hence the area of the beam of emission, is 1 mm^2. This value, along with others in the table, were used to calculate the radiant emittance and power of the signal entering the MCT detector. The power of the emission, $8.9 \times 10^{-7} W$ is well within the range of detectable signals for the ThorLabs MCT detector.

These values assume that each piece of equipment is operating within nominal specifications. Upon measuring the laser diode power, it was discovered that it was not operating at full power, and therefore the sample was not being heated as expected. This is one reason the detector was not recording any emission from the sample. However, as it was discussed earlier, even with a properly functioning 400 mW laser, the MCT detector would not produce a voltage response high enough to meet the lower limit of the lock-in amplifier at ambient temperatures. The DC voltage produced for a 400 mW laser was calculated to be 66.7 nV. The lower limit for the LIA is 100 nV. While the detector can detect the emission from the sample, the LIA is then not able to lock-in to the output from the MCT detector, as it is just below its abilities.

5. CONCLUSION

5.1. SUMMARY

Modulated Photothermal Radiometry is an asset in determining the thermal transport properties of both non-irradiated and irradiated samples. This non-destructive technique is ideally suited for optically dense and conductive samples with or without surface layers, though the possibility of measuring diffusivity in layered structures gives the technique its advantages. The determination of the thermal diffusivity coefficient can help in the research, development, and selection of materials in applications where heat transfer is important. In nuclear materials research PTR specifically helps in thermal characterization of ion irradiated materials.

The objective of this study was to design, build and test a PTR system and perform tasks to support that goal. In the process, it was broken into sections. The first, building and assembling the system was accomplished without error. Secondly, aligning the equipment required a trial and error process of determining which parts worked well with the system. After the electro-optic modulator was found to be inoperative for the given laser or geometry, it was replaced with an optical chopper to accomplish the task of modulating the laser signal.

To ensure that the combination of laser, MCT detector and lock-in amplifier was suited to the measurement conditions, analytical and numerical calculations were performed to evaluate the PTR system and redesign parts of it if necessary. After this investigation, it was found that while a laser power of 400 mW should be sufficient to heat the sample enough to produce an emission signal detectable by a thermoelectrically-

cooled MCT detector, the voltage output from the detector was still below the lower limit detectable of the SR510 lock-in amplifier and near the limit for the SR830 lock-in amplifier. It was also discovered that the laser itself was not emitting 400 mW though this was easily fixed by replacing the laser.

5.2. RECOMMENDATIONS

After determining that the signal being emitted from the sample surface is indeed detectable by the ThorLabs MCT detector, but outside of the lock-in amplifier's limits, the following recommendations are made.

By increasing the laser power to 1 W, the change in temperature is increased to 0.005K. By increasing this laser to 1 W, the voltage output from both MCT detectors is shown in Table 5.1. While this provides a stronger signal than the sensitivity limit of the SR830 LIA, a 400 mW visible laser, being class 3b, requires considerably less safety infrastructure than a 1W (class 4) laser.

Table 5.1: Detector voltage response for a laser power of 1 W.

Detector	ΔT (K)	ΔdV_{peak} (300K)	ΔdV_{peak} (500K)
Judson J15D16	0.01048 K	81.87 µV	505 µV
Thorlabs PDA10JT	0.01048 K	341.1 nV	20.5 µV

For this reason, the Stanford Research Systems SR830 lock-in amplifier is suggested for use with the Judson liquid nitrogen cooled detector. The Judson detector is able to produce voltages that are easily detectable by the SR830 LIA and even the SR510

LIA. With the Judson detector, it would not be necessary to replace both the MCT detector and lock-in amplifier. Given the much lower cost of the Judson detector compared with the highest sensitivity lock-in amplifier (e.g. SR865A), the replacement of the detector should produce the most cost effective approach, additionally obviating the need to upgrade the power source to a class 4 laser. With a combination of these changes, it is believed that the system will then be able to produce accurate results that can be used to determine the thermal diffusivity of both unirradiated and irradiated samples.

APPENDIX A.

TEMPERATURE ESTIMATE SCRIPT

```
rhoc=3.868*10^6; % J/m^3-K  Figure out which units to use here and typical values for
inorganic oxides/metals
k=13.53; %Thermal conductivity. W/m-K..same here. Get the units and typical values
D=3.4978*10^-6; %Diffusivity of unirradiated SS316 m^2/s

power = 100; %Laser power in Watts  - increase
beam_radius = 1.5; %Beam radius in mm
beam_radius = beam_radius*3e-3; %Beam radius in m
beam_area = pi*beam_radius^2; %Beam area in m^2
q_laser = power/beam_area; %Continous laser power density W/m^2

chop_frequency = 20; %Hz....sort of the main dial for frequency dependence
point_cycle = 100; %points per cycle
no_cycles = 700; %number of cycles...enough to converge
delta_t = 1/chop_frequency/point_cycle;

time_index = linspace(0,point_cycle*no_cycles-1,point_cycle*no_cycles)'; %number of
steps you'll have
time = time_index*delta_t;%total time
q_laser_t = q_laser*(mod(time_index,point_cycle)<(point_cycle/2));

no_layers = 50; %Maybe move to top
delta_x = 0.1; %Layer thickness in mm...might want to change this as well
delta_x = delta_x*1e-3; %Layer thickenss in m

x_index = linspace(0,no_layers,no_layers+1);
x = delta_x*x_index;
T = 293.15*ones(point_cycle*no_cycles,no_layers+1); %initial temp of sample - room
temp

check=D*delta_t/delta_x^2; %Neumann stability criterion. If satisfied, will continue, if
not, will kill program
if check>=0.5
   disp('Neumann criterion not satisfied')
   return
end

for i=1:length(time_index)-1

T(i,1) = T(i,2); %Adiabatic BC
T(i,no_layers+1) = 293.15; %Heat Sink BC

for j=2:no_layers
   if j==2
        T(i+1,j) = T(i,j)+delta_t/rhoc*(q_laser_t(i)+k*(T(i,j+1)-2*T(i,j)+T(i,j-
1))/delta_x^2);
```

```
    else
        T(i+1,j) = T(i,j)+delta_t/rhoc*(k*(T(i,j+1)-2*T(i,j)+T(i,j-1))/delta_x^2);
    end
end
end
filename='Temperatures.xlsx'
xlswrite(filename,T)

plot(time,T(:,2)-293.15);
xlabel('Time (s)')
ylabel('Temp(K)')
title('Temperature of Sample Surface')
```

APPENDIX B.

THORLABS PDA10JT SPECS

Thorlabs PDA10JT	
Wavelength Range	2.0 - 5.4 μm
Peak Wavelength (λ_p)	4.8 μm
Peak Responsivity	300 V/W (Typ.) at Peak Wavelength
Gain Settings	0, 4, 10, 16, 22, 28, 34, 40 dB (8 Steps)
Bandwidth Settings	1.25, 2.5, 5, 10, 20, 40, 80, or 160 kHz (8 Steps)
Output Voltage[a]	0 - 5 V at 50 Ω 0 - 10 V at High Z
Output Impedance	50 Ω
Output Current	100 mA (Max)
Load Impedance	50 Ω to High Z
Output Offset[b]	20 mV (Typ.) 45 mV (Max)
TEC Temperature	-30 °C
TEC Current	0.6 A (Typ.) 1.0 A (Max)
Thermistor	10 kΩ
Detector Element	HgCdTe (MCT)
Active Area	1 mm × 1 mm
Surface Depth	0.11" ± 0.02" (2.90 ± 0.40 mm)
Output	BNC
Detector Size	3" × 2.2" × 2.2" (76.2 mm × 55.9 mm × 55.9 mm)
Weight	Detector: 0.42 lbs (191 g) Power Supply: 2.1 lbs (955 g)
Power Supply	31 W, Location-Specific Power Cord Included
Input Power	100 - 120 VAC, 50 - 60 Hz (-EC Version: 220 - 240 VAC)
Gain (High Z)[c]	
0 dB	0.8 V/V
4 dB	1.6 V/V
10 dB	3.2 V/V
16 dB	6.3 V/V
22 dB	12.6 V/V
28 dB	25.2 V/V
34 dB	50.1 V/V

40 dB	100 V/V
Noise-Equivalent Power (NEP) Values[d]	
0 dB	1.90×10^{-9} W/Hz$^{1/2}$
4 dB	1.19×10^{-9} W/Hz$^{1/2}$
10 dB	5.94×10^{-10} W/Hz$^{1/2}$
16 dB	3.02×10^{-10} W/Hz$^{1/2}$
22 dB	1.51×10^{-10} W/Hz$^{1/2}$
28 dB	7.61×10^{-11} W/Hz$^{1/2}$
34 dB	3.86×10^{-11} W/Hz$^{1/2}$
40 dB	2.08×10^{-11} W/Hz$^{1/2}$

a. Saturation of the output voltage may cause damage to the HgCdTe (MCT) detector element.
b. Offset after the temperature has stabilized at each gain step. The worst-case offset is for the 40 dB gain step.
c. The gain for a 50 Ω impedance is one-half of the gain for high Z.
d. Measured at λ_p with a 160 kHz bandwidth and a 50 Ω impedance.

APPENDIX C.

TELEDYNE JUDSON J15D16 SPECS

Teledyne Judson J15D16	
Active Size	1 mm
Cutoff Wavelength, I_{co}	~16.6 μm (600cm-1)
Peak Wavelength, I_{peak}	~14 μm
Peak Detectivity, D* @ 10 kHz	Min. $2.5 \times 10^{10}\ cm\ Hz^{1/2}W^{-1}$ Typ. $3\times 10^{10}\ cm\ Hz^{1/2}W^{-1}$
Typical Responsivity @ I_{peak}	900 V/W
Time Constant, t	0.3 μsec
Typical Resistance, RDET	18 to 120 W/sq
Typical Bias Current IB	~30 mA

BIBLIOGRAPHY

[1] Olander, D.R. “Fundamental Aspects of Nuclear Reactor Fuel Elements” *United States: N.p.,* 1976. doi:10.2172/7343826

[2] Alter Technology Tüv Nord, “Displacement Damage – ALTER TECHNOLOGY”, *Web Project Office, 23 April. 2018,* https://wpo-altertechnology.com/displacement-damage-testing/

[3] Dongliang Zhao, Xin Qian, Xiaokun Gu, Saad Ayub Jajja, Ronggui Yang, “Measurement Techniques for Thermal Conductivity and Interfacial Thermal Conductance of Bulk and Thin Film Materials” *Department of Mechanical Engineering, University of Colorado, Boulder, 2016*

[4] Francis Weston Sears, Gerhard L. Salinger, “Thermodynamics, Kinetic Theory, and Statistical Thermodynamics.”, *Addison-Wesley Publ., pp. 80-81.* 1986

[5] L. Fabbri and P. Fenici, “Three-dimensional Photothermal Radiometry for the Determination of the Thermal Diffusivity of Solids,” *Review of Scientific Instruments 66,* 1995

[6] Libor Vozár, Wolfgang Hohenauer, “Flash Method of Measuring the Thermal Diffusivity. A Review,” *High Temperatures-High Pressures, vol 35/36, pp 253-264,* 2003/2004

[8] Chris Dames, “Measuring the Thermal Conductivity of Thin Films: 3 Omega and Related Electrothermal Methods”, *Department of Mechanical Engineering, University of California at Berkely, 2013*

[9] Peter Ŝuŝnjar, as.prof.dr.Boris Majaron, “Pulsed Photothermal Radiometry,” *Univerza v Ljubljani,* 2014

[10] A Mandelis, R.A. Budiman, M. Vargas, and D. Wolff, “Noncontact Photothermal Infrared Radiometric Deep-level Transient Spectroscopy of GaAs Wafers,” *Applied Physics Letters 67,* 1995

[11] Luka Vidovic, Matija Milanic, Lise Lyngsnes Randeberg, Boris Majaron, “Quantitative characterization of traumatic bruises by combined pulsed photothermal radiometry and diffuse reflectance spectroscopy.” *Progress in Biomedical Optics and Imaging - Proceedings of SPIE. 9303. 10.1117/12.2077188,* 2015

[12] Per-Erik Nordal and Svein Otto Kanstad “Phothermal Radiometry,” *Physica Scripta, vol. 20 pp.659-662,* 1979.

[13] Murdin, P, "Encyclopedia of Astronomy and Astrophysics", *Article ID 4598, Bristol: Institude of Physics Publishing, 2001*

[14] Erno Pungor, "A Practical Guide to Instrumental Analysis," *Florida: Boca Raton pp. 181-191,* 1995

[15] "HgCdTe (MCT) Amplified Photodetector with TEC." *Thorlabs,* www.thorlabs.com/newgrouppage9.cfm?objectgroup_id=2907.

[16] A. Salnick, A. Mandelis, and C. Jean, "Infrared Photothermal Radiometric Deep-level Transient Spectroscopy of Shallow B^+ Dopant States in p-Si," *Applied Physics Letters,* 1997

[17] Agustín Salazar, Raquel Fuente, Estibaliz Apiñaniz, Arantza Mendioroz, and R. Celorrio, "Simultaneous Measurement of Thermal Diffusivity and Optical Absorption Coefficient Using Photothermal Radiometry. II Multilayered Solids," *Journal of Applied Physics, 110,* 2011

[18] B. Schmitz and G. Goch, "Photothermal Radiometry – Principle and Applications," *ILM, Lasermeßtechnik, Ulm,* 2000

[19] Andrzej Kusiak, Jiri Martan, Jean-Luc Battaglia, and Rosislab Daniel, "Using Pulsed and Modulated Photothermal Radiometry to Measure the Thermal Conductivity of Thin Films," *Thermochimica Acta 556,* 2013

[20] Nolwenn Fleurence, Bruno Hay, Guillaume Davée, Andréa Cappella, and Emilie Foulon, "Thermal Conductivity Measurements of Thin Films at High Temperature Modulated Photothermal Radiometry at LNE," *Physica Status Solidi, Vol. 212, Issue 3,* 2015

[21] Thorlabs, *Thermoelectric Temperature Controller Operation Manual, pp 1,* 2017

[22] Thorlabs, *Optical Chopper User Guide, pp 3,* 2016

[23] Thorlabs, *Si Biased Detector User Guide pp 2,* 2017

VITA

Jessica Nicole Seals was born in Mission, Kansas. Jessica previously earned her Bachelor of Science in Nuclear Engineering from Missouri University of Science and Technology in 2016. In December of 2018, she received her Master of Science in Nuclear Engineering from Missouri University of Science and Technology.